Bull Volcanol (2002) 64:486–501
DOI 10.1007/s00445-002-0230-5

RESEARCH ARTICLE

C. Klug · K.V. Cashman · C.R. Bacon

Structure and physical characteristics of pumice from the climactic eruption of Mount Mazama (Crater Lake), Oregon

Received: 5 November 2001 / Accepted: 24 April 2002 / Published online: 26 June 2002

Abstract The vesicularity, permeability, and structure of pumice clasts provide insight into conditions of vesiculation and fragmentation during Plinian fall and pyroclastic flow-producing phases of the ~7,700 cal. year B.P. climactic eruption of Mount Mazama (Crater Lake), Oregon. We show that bulk properties (vesicularity and permeability) can be correlated with internal textures and that the clast structure can be related to inferred changes in eruption conditions. The vesicularity of all pumice clasts is 75–88%, with >90% interconnected pore volume. However, pumice clasts from the Plinian fall deposits exhibit a wider vesicularity range and higher volume percentage of interconnected vesicles than do clasts from pyroclastic-flow deposits. Pumice permeabilities also differ between the two clast types, with pumice from the fall deposit having higher minimum permeabilities (~5×10^{-13} m^2) and a narrower permeability range ($5–50\times10^{-13}$ m^2) than clasts from pyroclastic-flow deposits ($0.2–330\times10^{-13}$ m^2). The observed permeability can be modeled to estimate average vesicle aperture radii of 1–5 μm for the fall deposit clasts and 0.25–1 μm for clasts from the pyroclastic flows. High vesicle number densities (~10^9 cm^{-3}) in all clasts suggest that bubble nucleation occurred rapidly and at high supersaturations. Post-nucleation modifications to bubble populations include both bubble growth and coalescence. A single stage of bubble nucleation and growth can account for 35–60% of the vesicle population in clasts from the fall deposits, and 65–80% in pumice from pyroclastic flows. Large vesicles form a separate population which defines a power law distribution with fractal dimension D=3.3 (range 3.0–3.5). The large D value, coupled with textural evidence, suggests that the large vesicles formed primarily by coalescence. When viewed together, the bulk properties (vesicularity, permeability) and textural characteristics of all clasts indicate rapid bubble nucleation followed by bubble growth, coalescence and permeability development. This sequence of events is best explained by nucleation in response to a downward-propagating decompression wave, followed by rapid bubble growth and coalescence prior to magma disruption by fragmentation. The heterogeneity of vesicle sizes and shapes, and the absence of differential expansion across individual clasts, suggest that post-fragmentation expansion played a limited role in the development of pumice structure. The higher vesicle number densities and lower permeabilities of pyroclastic-flow clasts indicate limited coalescence and suggest that fragmentation occurred shortly after decompression. Either increased eruption velocities or increased depth of fragmentation accompanying caldera collapse could explain compression of the pre-fragmentation vesiculation interval.

Editorial responsibility: M. Rosi

C. Klug · K.V. Cashman (✉)
Department of Geological Sciences,
University of Oregon, Eugene, OR 97403-1272, USA
e-mail: cashman@oregon.uoregon.edu

C.R. Bacon
U.S. Geological Survey, 345 Middlefield Rd.,
MS 910, Menlo Park, CA 94025-3591, USA

Introduction

Explosive silicic eruptions produce large quantities of pumice and ash by processes of vesiculation and fragmentation that are not well understood. Recent work on the relationship between magmatic vesiculation and fragmentation can be summarized using two end-member models (e.g., Cashman et al. 2000). In the first, vesiculation provides the driving force for magma expansion and acceleration and fragmentation results from high strain rates in the rapidly expanding mixture. In this scenario, clasts may form from fluid instabilities, or by brittle failure if the tensile strength of the magma is exceeded. In the second model, fragmentation of an already vesiculated magma occurs by sudden decompression. Here fragmentation occurs in response to downward propagation of an unloading wave in the melt, or through layer-by-layer unloading of pressurized bubbles as a fragmentation wave travels through the expanding gas (Alidibirov

and Dingwell 2000). The first mechanism, with disruption by fluid instabilities, seems the likely cause of fragmentation in Hawaiian fire fountains, whereas the second mechanism probably prevails in the explosive disruption of highly viscous domes.

Fragmentation in large-volume silicic eruptions may involve both processes. Disruption of the liquid may accompany vesiculation and resultant acceleration of the bulk magma to produce a range of clast sizes (pumice). The extent to which these clasts continue to expand after fragmentation (Thomas et al. 1994; Kaminski and Jaupart 1997) is not well constrained. The limited range in pumice permeability observed in Plinian fall deposits (~10^{-12} m^2; Klug and Cashman 1996; Tait et al. 1998) suggests that preservation, rather than disruption, of larger clasts may require that a threshold permeability be reached. Fine ash (<63 μm) may result from rapid decompression of individual overpressured bubbles (Sparks 1978) or by pulverization of quenched clasts within the conduit (Kaminski and Jaupart 1998). Either process could explain the observed increase in the volumetric proportion of fine ash with increasing eruption intensity (mass flux; e.g., Walker 1973).

Recent experimental studies of bubble nucleation and growth in rhyolitic melts provide a new framework for studying vesiculation in natural systems. Of primary importance is the observation that homogeneous bubble nucleation occurs only under conditions of large supersaturations (ΔP>120–150 MPa; Hurwitz and Navon 1994; Mourtada-Bonnefoi and Laporte 1999; Mangan and Sisson 2000), whereas heterogeneous nucleation on preexisting microlites may occur at ΔP<20 MPa (Hurwitz and Navon 1994; Gardner et al. 1999). Although maximum rates of bubble nucleation are poorly constrained by experiments, minimum rates of homogeneous and heterogeneous nucleation are similar at similar rates of decompression, leading Mangan and Sisson (2000) to conclude that although the presence or absence of heterogeneities plays an important role in degassing efficiency, nucleation rates (and resulting bubble number densities) are most strongly controlled by the rate of depressurization. The spatial density of bubble nuclei, in turn, controls rates of diffusion-limited bubble growth (Lyakhovsky et al. 1996; Proussevitch and Sahagian 1998; Liu and Zhang 2000), and growth of volatile depletion shells around individual bubbles (e.g., Zhang 1999; Lensky et al. 2001).

Vesicle textures in pumice clasts preserve information on the integrated process of magmatic vesiculation during ascent and fragmentation. To relate textures to conditions of pumice formation, we examine clasts produced during both Plinian fall and pyroclastic flow-producing phases of the climactic eruption of Mount Mazama (Crater Lake), Oregon. We do not attempt a statistical characterization of the variation in pumice clast textures within each stratigraphic horizon of the fall and flow deposits. Rather we seek to catalog features that provide information on processes occurring during the ascent, vesiculation, and fragmentation of magma throughout the eruptive sequence and to determine which, if any, features of the clasts reflect changes in the physical conditions of eruption. As characterization of vesicle sizes and shapes in a single sample is time-consuming, a secondary goal of this study is to test the sensitivity of easily measured bulk properties (vesicularity, permeability; ~50 samples) to variations in internal pumice structure, as characterized by the more labor-intensive image analysis (10 samples).

Methods

Geologic background and sample collection

Crater Lake formed about 7,700 years ago during the climactic eruption of ~50 km^3 of magma from Mount Mazama. The eruption can be divided into two phases (Bacon 1983): (1) a *single-vent phase* which produced a Plinian fall deposit separable into two parts (the Lower and Upper pumice of Young 1990), and the pyroclastic flows of the Wineglass Welded Tuff, and (2) a *ring-vent phase*, in which a compositionally zoned pyroclastic-flow deposit was generated from multiple vents around the subsiding caldera floor. Most of the erupted volume is hydrous rhyodacitic pumice (70.4±0.2 wt% SiO_2 anhydrous, Bacon and Druitt 1988; 3.9 wt% pre-eruptive H_2O dissolved in the melt, Bacon et al. 1992), with minor basaltic to andesitic scoria comprising only the upper part of the ring-vent-phase ignimbrite (Druitt and Bacon 1986, 1989).

The stratigraphy of climactic Mazama deposits is well documented (e.g., Williams 1942; Bacon 1983; Druitt and Bacon 1986; Young 1990). The climactic fall deposit (CP samples in Table 1) is up to 20 m thick along the northern part of the caldera rim and easy access permits sampling throughout this deposit (Fig. 1). Most notable is the prevalence of large (15–20 cm) pumice clasts with abundant elongate vesicles in the uppermost part of the Plinian fall deposit. The Wineglass Welded Tuff (WT) is incipiently to densely welded but contains several lithic-rich layers in which welding is less intense (Kamata et al. 1993). One such layer at the eastern edge of a middle Wineglass Welded Tuff flow unit provides an unusual opportunity to examine post-emplacement changes in pumice structure that accompany slow cooling within a rapidly accumulating deposit (changes which likely preceded welding throughout much of the deposit). Pumice clasts within this layer are large (>20 cm) and most have highly elongate vesicles. The pyroclastic flow from the ring-vent phase (PF) is non-welded to indurated or partly welded and is well exposed in canyons around Mount Mazama such as at The Pinnacles (Fig. 1). The base of the deposit is dominated by rhyodacitic pumice that is compositionally indistinguishable from pumice erupted during the preceding, single-vent phase of the eruption. Pumice clasts from this location are unusual in comparison with the fall deposits in their fine-scale vesicularity.

Table 1 Description and measurements of Crater Lake pumice clasts

Eruption phase and deposit[a]		Relative location	Sample name	Texture[b]	Mode of vol. dist. (μm)	Vol.-based median (μm)	N^m_V (log no. cm^{-3})	Average permeability (m^2)	Vesicularity		No. cores[c]
									Bulk (%)	Con-nected (%)	
Ring vent	PF	Base	PF15	S, C, R, E	20	28	10.34	2.6×10^{-13}	78.2	70.6	9
			PF15edge		16	28	10.03				
			PF15d		20	22	10.00				
			PF15L		20	25	10.05				
Single vent	WT	Near base	WT9	L, C, H	13	20	10.46	5.2×10^{-12}	79.5	76.7	8
			WT9v		20	28	10.13				
			WT9L		16	16	10.27				
	CP	Near top	CP10	S, C	50	42	9.78	2.0×10^{-12}	78.5	76.4	5
			CP12	S, C	–	–	–	8.3×10^{-13}	84.3	80.8	1
			CP11	D, C, R	40	40	9.60	1.1×10^{-12}	81.4	80.4	1
		Middle	CP14	D, C, R	5,012	200	8.56	7.3×10^{-13}	85.0	82.4	4
			CP8	S, C, R	–	–	–	1.2×10^{-12}	83.9	83.0	3
			CP7	S/D, C	–	–	–	8.1×10^{-13}	79.7	76.3	3
		Base	CP5	S, C	32	71	9.69	4.4×10^{-13}	80.8	76.4	2

[a] Each sampling location is given a separate number with a prefix designating whether the location is in the Plinian fall (*CP*), Wineglass Welded Tuff (*WT*) or ring-vent-phase pyroclastic-flow (*PF*) deposit. Several clasts were collected from each site. These are distinguished only for the WT and PF locations where different clasts were examined along (*L*) and perpendicular to the direction of vesicle elongation in clasts with tube vesicles. Unusually dense (*d*) and vesicular (*v*) clasts were also imaged separately, as was the edge of one PF clast. Textural descriptions are based on qualitative observations of SE and BSE images. Primary modes of the volume distributions are from Fig. 8, volume-based medians from Fig. 9. Melt-referenced vesicle number densities (N^m_d), permeabilities, and vesicularities are as described in text

[b] Characteristic textural features include *S* Spherical vesicles, *D* deformed vesicles, *L* elongate vesicles, *N* narrow size range, *C* large coalesced cavities, *R* extensive melt film wrinkling, *H* highly retracted melt films, *E* differential expansion

[c] Number of cores averaged for permeability and vesicularity measurements

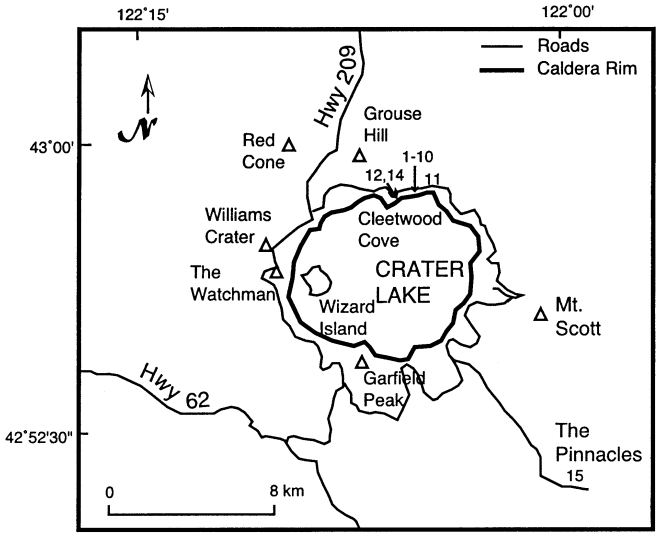

Fig. 1 Sample location map; locations are shown by *numbers* and *arrows* (described in text)

Sample characterization

Density (vesicularity) and permeability were determined for all samples. These bulk measurements were used to select samples for more detailed textural analysis.

Vesicularity and permeability

Pumice clast vesicularities were measured using a multivolume He-pycnometer (as described in Klug and Cashman 1994). Pumice clasts were cut into 25-mm-diameter cores and the total He non-accessible volume was determined using the pycnometer. As this volume can include isolated pores, solid densities were determined for powders of six separate samples; each yielded a density of 2,400 kg m^{-3}. This solid density was used, together with the core volume, to calculate the bulk vesicularities of all other samples. The difference between the He-pycnometry vesicularity and the bulk vesicularity is a measure of the volume percentage of isolated (He-inaccessible) vesicles.

Pumice permeability was measured on the same samples at Stanford University using a Ruska gas permeameter with nitrogen as the working gas (e.g., Klug and Cashman 1996). Core dimensions of 25-mm diameter and 32-mm length are 5–10 times larger than the largest vesicles and we assume that measured permeabilities are representative of the entire clast. Three measurements were made on each sample, with samples removed from the holder, flipped end for end, and re-inserted between each run. Average standard deviations for these three measurements were 4.5%. Determining the extent to which the measured permeabilities are representative of the vesicle structure (and not cooling-related fractures) is one goal of this study.

Vesicle size measurements

Pumice clasts are commonly heterogeneous on the scale of a single thin section and contain vesicles which span several orders of magnitude in size (<1 μm^2 to >50 mm^2). For this reason, analysis of clast textures requires several complementary strategies. Whole-clast assessment of vesicle size, shape, interconnectivity, and morphology is provided by secondary electron (SE) images obtained by means of a scanning electron microscope (SEM). We use a JEOL JSM-6300 V SEM and 0.5 kV accelerating voltage to image fresh pumice surfaces without excessive sample charging. Thin sections (impregnated with the low viscosity epoxy Epofix) are imaged using backscattered electrons (BSE) to view details of vesicle size, shape and wall thickness. To measure the full range of vesicle sizes, additional images are collected at low magnification using a petrographic microscope and scans of entire thin sections.

Images are processed and analyzed using Adobe Photoshop and NIH Image 1.60 software. We measure 3,000–7,500 vesicles per thin section, depending on clast heterogeneity, and one to three clasts from each sample location. Binary images produced by gray scale thresholding usually require manual editing prior to automated measurement of vesicle area, shape, and wall thickness. In particular, thin bubble walls disappear during image acquisition and processing, and must be redrawn. Additionally, individual vesicles show a sufficiently high degree of interconnectivity that it is necessary to reconnect ('decoalesce') partially ruptured (incompletely retracted) bubble walls (e.g., Klug and Cashman 1994, 1996). Measured vesicle characteristics thus represent the state of the magma just prior to the last discernible stage of bubble coalescence.

Three-dimensional size distributions are defined by calculating equivalent diameters (L) from vesicle area measurements, binning to determine areal number densities for each vesicle diameter size (N_A), and converting to a three-dimensional distribution (number per volume, N_V) assuming $N_V=N_A/L$ (Klug and Cashman 1994). This conversion corrects for the 'intersection probability' by designating sampling planes which are proportional to vesicle size (Underwood 1970). Total vesicularity is calculated by summing vesicle volumes represented by each size range. For pumice clasts with highly elongate vesicles, thin sections are cut parallel and perpendicular to the direction of elongation to estimate appropriate aspect ratios for the volume conversion. All other vesicles are treated as spheres, and the vesicle diameter that of a sphere of equal volume. Summed vesicle volume distributions typically yield total vesicularities which are 10–20% lower than measured vesicularities, a consequence of intersecting most vesicles at an apparent diameter smaller than the true diameter (e.g., Cashman and Marsh 1988). We use the vesicularity discrepancy to determine a constant by which the vesicle distribution can be corrected for this 'cut effect'.

An alternative method of two-dimensional to three-dimensional conversion, based on a geometric binning scheme (appropriate for lognormal distributions) and sectioning of spherical vesicles, has been suggested by Sahagian and Proussevitch (1998). A comparison of our method with that of Sahagian and Proussevitch shows only minor differences in estimated vesicle volume distributions (Fig. 2). We have chosen to use the simpler N_A/L conversion because it permits more flexibility in definition of vesicle size ranges, does not require an assumption of vesicle shape, and uses the independent measurement of bulk vesicularity as an additional constraint. This latter constraint is particularly important for heterogeneous samples, for which truly representative images of the clast structure are difficult to obtain at all scales.

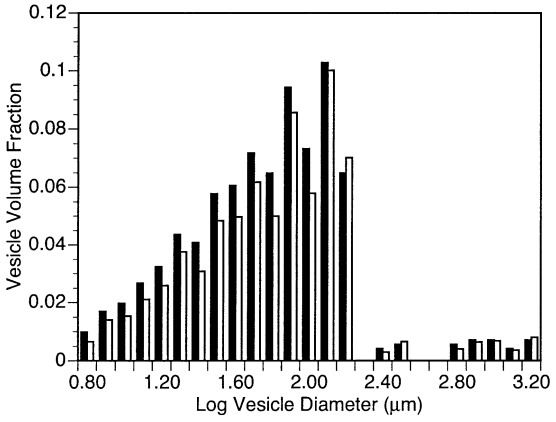

Fig. 2 Comparison of N_A and N_V conversion methods. *Open bars* are method of Sahagian and Proussevitch; *closed bars* are method used in this study

Results

Vesicularity and permeability

The bulk vesicularity of all pumice clasts is high (75 to 88%; Fig. 3), as is common in many silicic pyroclastic deposits (Houghton and Wilson 1989; Cashman and Mangan 1994; Gardner et al. 1996; Polacci et al. 2001), and all clasts have high pore interconnectivity (>90 vol%). In detail, Plinian fall samples have the widest range in bulk vesicularity. As Mazama magma was phenocryst poor (<10%; Druitt and Bacon 1989), measured vesicularities are approximately those of the melt. Clasts from the fall deposit also have a relatively high degree of bubble connectivity, with most of the samples having <~4 vol% isolated pores (Fig. 3). By contrast, pumice samples from pyroclastic flows comprising the Wineglass Welded Tuff and ring-vent-phase ignimbrite have a narrower vesicularity range and slightly lower bulk vesicularities (75–81%). However, long-tube pumice clasts from the Wineglass Welded Tuff have consistently small proportions of isolated pores (2–3 vol%), whereas samples from pyroclastic flows of the ring-vent phase show a marked increase in isolated pore volume (5–10 vol%).

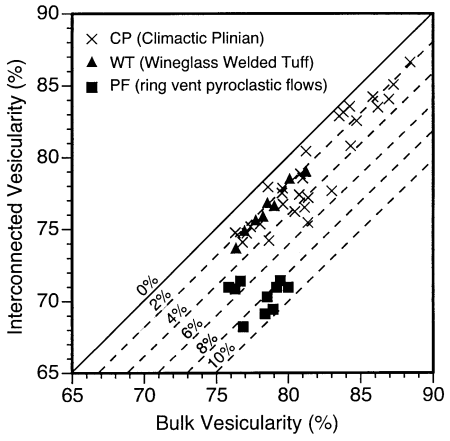

Fig. 3 Comparison of pumice vesicularity determined by He-pycnometry and calculated using the solid volume and a solid density of 2,400 kg m^{-3}. *Dashed lines* show contours of the volume percentage of isolated vesicles

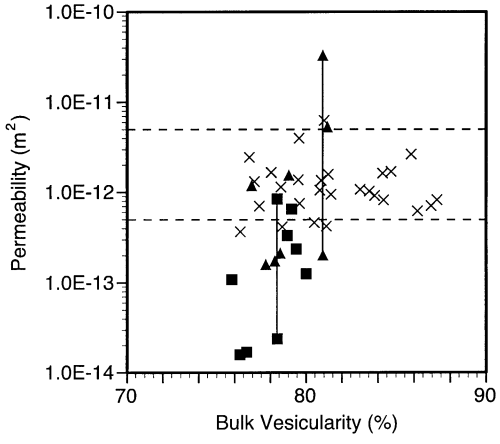

Fig. 4 Relationship between pumice vesicularity and permeability in all Crater Lake pumice samples. *Symbols* are the same as in Fig. 3. *Dashed lines* show range of typical Plinian pumice permeabilities (from Klug and Cashman 1996). Vertical *tie lines* link permeability measurements made parallel (high values) and perpendicular (low values) to directions of vesicle elongation in long-tube pumice clasts

Measured permeabilities show no simple relationship to clast vesicularity (Fig. 4). Pumice clasts from the Plinian fall deposits span a wide range of bulk vesicularities but have similar permeabilities ($0.5–5.0\times 10^{-12}$ m^2), a permeability range characteristic of pumice from many fall deposits (Klug and Cashman 1996; Gilbert and Sparks 1998; Tait et al. 1998; Saar and Manga 1999). By contrast, clast permeability in long-tube pumice from the Wineglass Welded Tuff is highly variable (10^{-13} to 3×10^{-11} m^2) over a relatively small range in vesicularity (78–81%), reflecting a strong permeability anisotropy in clasts with highly elongate vesicles. Pumice clasts from the ring-vent-phase ignimbrite have uniformly low permeabilities ($0.2–8\times10^{-13}$ m^2), even when vesicles are somewhat elongate. Low clast permeabilities may reflect the lower degree of vesicle connectivity determined from He-pycnometry (Fig. 3).

Pumice textures – qualitative observations

Images of whole pumice clasts and thin sections provide an overview of textural heterogeneities, bubble-bubble interactions, and bubble deformation styles that aids interpretation of vesicle size measurements and helps to constrain the processes which occur during ascent, vesiculation, and fragmentation of silicic magma. Of particular interest are mechanisms and extent of bubble coalescence (Klug and Cashman 1996), evidence for high strain rates (Marti et al. 1999), evidence of post-fragmentation expansion of pumice clasts (Thomas et al. 1994), and indications of the extent to which bubbles are inherited from the magma storage area (Whitham and Sparks 1986). Additionally, these images allow estimates of the critical melt film thickness required for coalescence (Cashman and Mangan 1994) and the range in pore aperture size controlling permeability (Saar and Manga 1999).

Whole-clast imaging

Pumice clasts show a wide variety of textural features. At one end of the spectrum are clasts with a narrow range of vesicle sizes and a predominance of small (10–20 μm), nearly spherical vesicles (Fig. 5a). At the other extreme are clasts with a wide range of vesicle sizes, including large cavities formed by the coalescence of several bubbles (Fig. 5b). Bubble deformation is typically heterogeneous, with isolated regions of aligned and elongated vesicles in a matrix of spherical vesicles. Localized deformation in shear zones tens to hundreds of μm in width suggests extensive shear localization in these highly vesicular samples. More uniform bubble elongation characterizes ‘long-tube’ pumice, although even these clasts can preserve evidence of multiple stages of deformation, as seen in refolded packets of small (<10 μm diameter) tube vesicles (Fig. 5c and inset).

All stages of bubble coalescence are preserved in Mazama pumice. Coalescence initiation can be seen where small bubbles expand into adjacent larger cavities (Fig. 5d). Subsequent wall rupture leaves pore apertures ~2–10 μm in diameter, some of which show wrinkling (‘parachute instabilities’; Debregeas et al. 1998) in response to release of gas overpressure (Fig. 5d). More extensive film retraction results in smooth pore apertures or delicate filaments (remnant interstices) which span coalesced cavities (Fig. 5e). Both extensive wrinkling and incomplete wall retraction are prevalent in pumice clasts from the upper fall deposit. Pumice clasts from a nonwelded unit of the Wineglass Welded Tuff show complete melt film retraction around the interior of large coalesced cavities (Fig. 5f). The unusually smooth interior texture of the clast shown in Fig. 5f (and inset) proba-

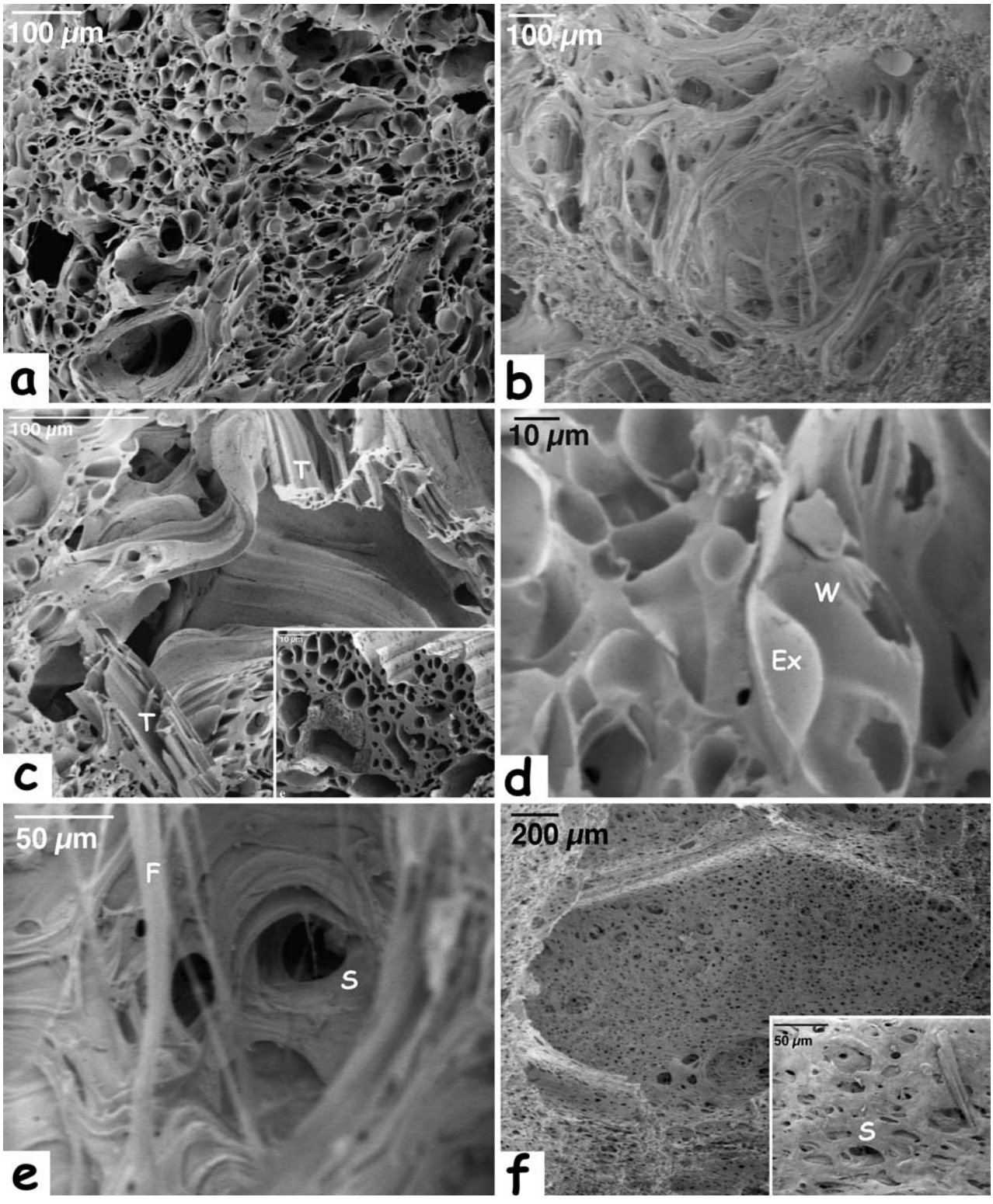

Fig. 5a–f SE images of Crater Lake pumice. **a** Narrow vesicle size range of CP5. **b** Large vesicle size range in PF15. **c** Deformed tube vesicles of CP7. **d** Expanding bubbles with wrinkled partial melt retraction films of CP11. **e** Smooth retraction and remnant filamentous interstices in PF15. **f** Extreme melt retraction and smooth interior walls of WT9. Features identified include deformed packets of tube vesicles (*T*), wrinkling around vesicle apertures (*W*), small bubbles expanding into larger cavities (*Ex*), smooth apertures (*S*), and remnant filament-like melt films (*F*)

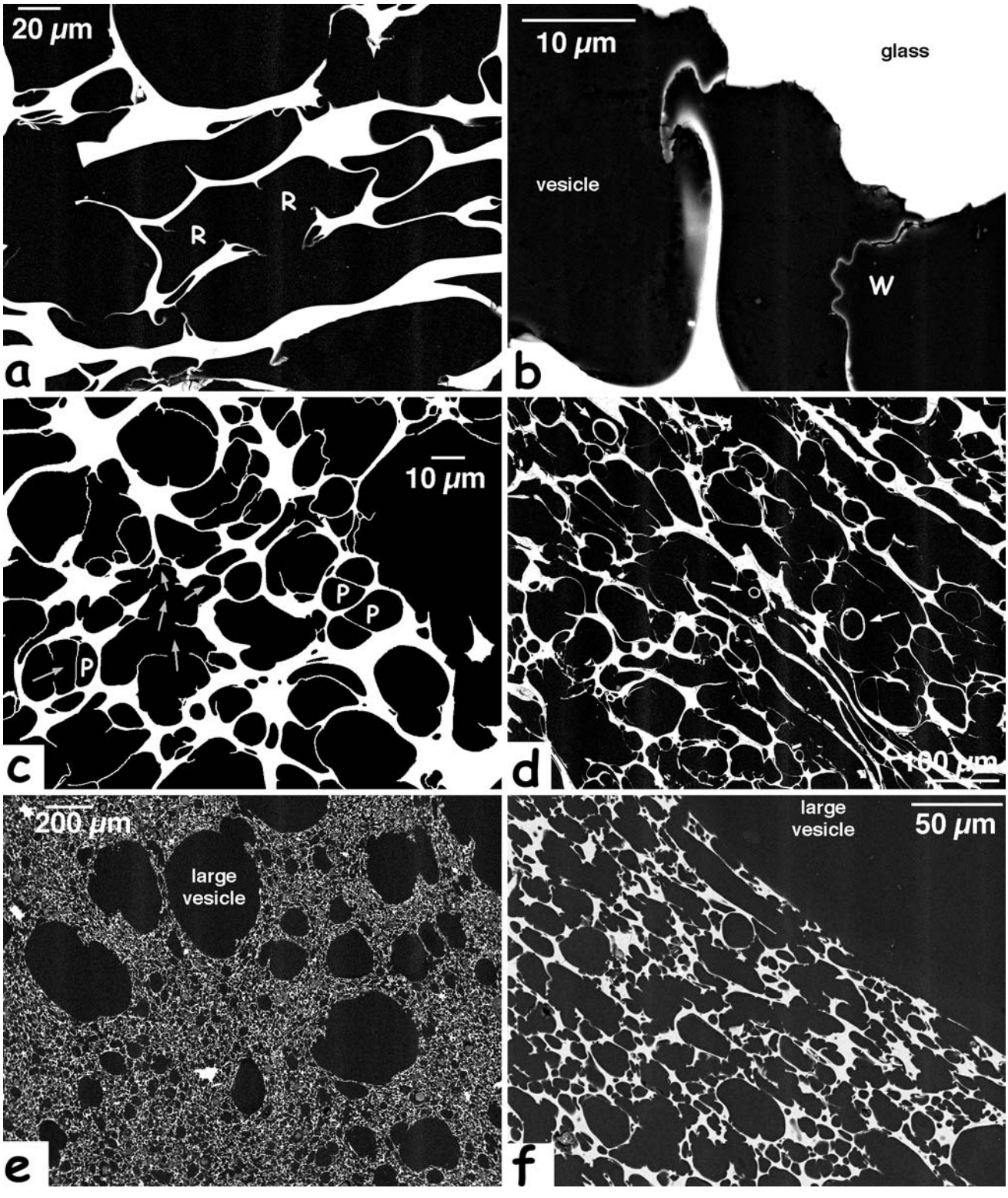

Fig. 6a–f BSE images of Crater Lake pumice. **a** Wrinkling of thin melt films in CP14. **b** Wrinkling of very thin melt films in PF15. **c** Flat films developed between bubbles of the same size, and sequential rupture of melt films (shown by *arrows*) in CP11. **d** 'Donut-like' two-dimensional evidence of small bubble expansion into larger cavities (shown by *arrows*) in CP14. **e** Perpendicular view of long-tube pumice of WT9. **f** Close-up of **e**, showing small vesicle deformation in response to radial expansion of large vesicles. Features identified include planar films (*P*) and locations of melt film retraction (*R*)

bly reflects slow cooling as a consequence of the rapid accumulation that led to welding of most of the deposit and provides the only example of extensive post-fragmentation modification of clast textures that we have identified.

Thin-section imaging

Conditions leading to bubble coalescence are best constrained by BSE (two-dimensional) images, where the failure of melt films can be directly related to film thickness. In general, melt films that exceed ~5–10 μm in thickness are stable. Bubble walls with a thickness of 1–5 μm are often deformed but have not failed completely, whereas films of <1 μm fail by either rupture and retraction, or rupture and wrinkling (Fig. 6a, b). Where bubbles of approximately similar sizes interact, separating films are planar and stable, even when ~1 μm thick (Fig. 6c). Rupture in this situation requires either continued film thinning to much less than 1 μm (Fig. 6b) or a change in the pressure gradient between adjacent bubbles (which increases the rate of film thinning; e.g., Klug and Cashman 1996; Mangan and Cashman 1996). Because a change in pressure gradient is most easily achieved by the change in the relative size of adjacent bubbles (e.g., Sparks 1978), a single coalescence event may trigger coalescence of adjacent bubbles (arrows in Fig. 6c). Additionally, small bubbles commonly expand into adjacent large cavities (e.g., Fig. 5d and the thin-section equivalent, seen as the donut-like features indicated by arrows in Fig. 6d).

Long-tube pumice clasts from the Wineglass Welded Tuff show multiple nucleation events and deformation regimes. Large (50–500 μm diameter) vesicles are highly elongated and impart a pronounced fabric to the pumice clasts (shown perpendicular to the elongation direction in Fig. 6e). Here elongated vesicles are surrounded by a matrix of small vesicles (<20 μm) that show little deformation in the elongation direction but are flattened around the large tube vesicles, apparently in response to late-stage radial expansion (Fig. 6f; equivalent to mesh-like structure in Fig. 5f).

Summary of qualitative observations

Mazama pumice clasts have vesicle populations that span a large size range and exhibit substantial variations in the extent of bubble deformation, coalescence, and post-coalescence melt film retraction. These variations can be broadly characterized in the context of deposit type. Pumice clasts from the Plinian fall deposit are heterogeneous and most clasts show extensive bubble coalescence. Wrinkling of partially retracted, bubble wall apertures suggests very late-stage coalescence (and viscous melt films) and is most common in samples from the middle of the climactic fall deposit (samples CP8, CP11, and CP14; Table 1). Pumice clasts from pyroclastic flows of the Wineglass Welded Tuff show late-stage radial expansion of large bubbles, complete retraction of coalescence apertures, and formation of mesh-like cavity walls. All of these features suggest post-emplacement modification of clast textures that is consistent with extensive welding in this deposit. Pumice clasts from pyroclastic flows of the ring-vent phase are locally heterogeneous, with large coalescence cavities separated by small vesicles. Where coalescence has occurred, bubble wall retraction is incomplete and wrinkling of very thin (~0.1 μm) walls is common.

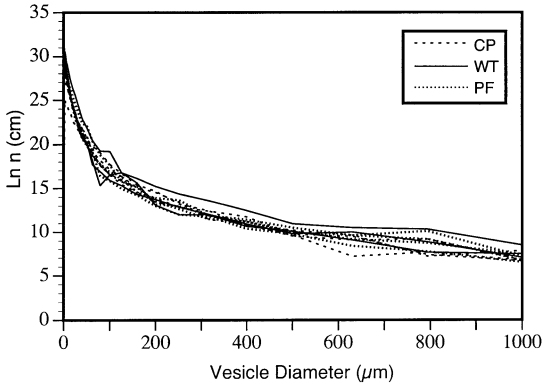

Fig. 7 Plot of vesicle size distributions (ln *n* vs. L) for pumice from the Plinian fall (*CP*), Wineglass Welded Tuff (*WT*) and ring-vent-phase pyroclastic-flow (*PF*) deposits

Quantification of vesicle textures

Vesicle textures are quantified to provide a basis for comparison among samples in this study and to relate Mazama pumice to other natural (e.g., Sparks and Brazier 1982; Whitham and Sparks 1986; Orsi et al. 1992; Klug and Cashman 1994, 1996; Polacci et al. 2001) and experimental (e.g., Hurwitz and Navon 1994; Mourtada-Bonnefoi and Laporte 1999; Gardner et al. 1999; Mangan and Sisson 2000) samples. Vesicle number densities (e.g., Toramaru 1990; Mangan et al. 1993; Klug and Cashman 1994; Mangan and Cashman 1996) provide information on bubble nucleation, and both vesicle volume and power law distributions of vesicle numbers (e.g., Gaonac'h et al. 1996a, 1996b; Simakin et al. 1999; Blower et al. 2001) can be used to quantify the extent of bubble coalescence.

Vesicle size distributions

Vesicle size distributions (VSDs) are calculated using the population number density *n*, defined as the slope of the cumulative number distribution dN/dL, where N is the vesicle number density per cm^3 and L is the vesicle size in cm. Linear relationships between ln *n* and L are common in crystallizing populations where the crystallization history is simple (constant rates of nucleation and

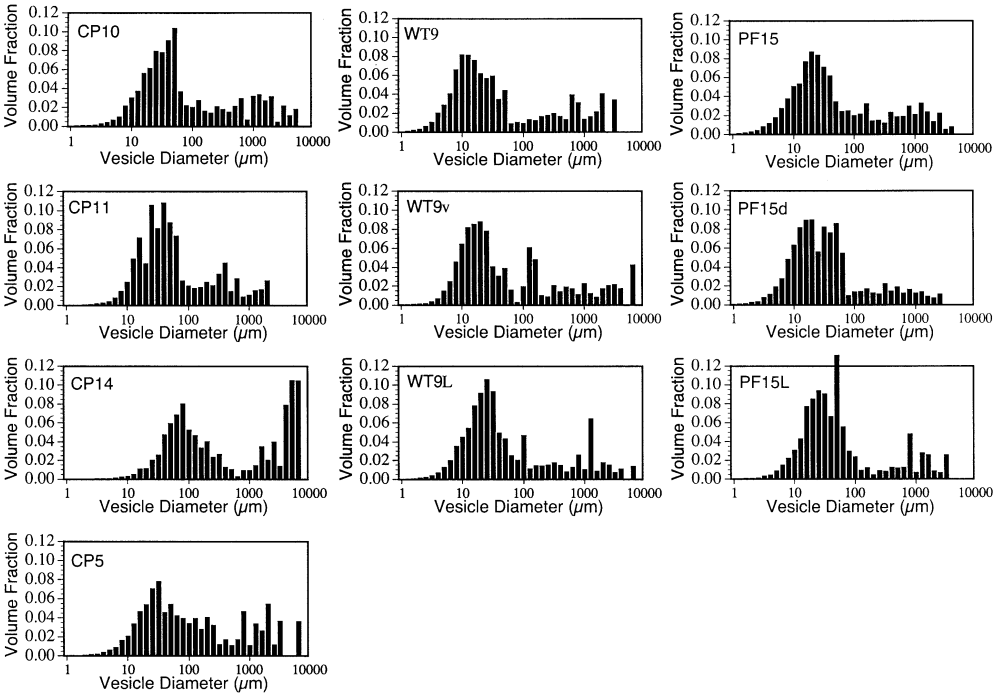

Fig. 8 Vesicle volume distributions of all pumice clasts. WT9v is a highly vesicular clast of WT9; PF15d is a dense clast of PF15. *L* Elongate vesicles

growth) and permit calculation of the dominant size and number density (per unit volume) of the population. Unfortunately, plots of ln *n* vs. L are extremely non-linear in all pumice clasts examined (Fig. 7), as anticipated given the qualitative evidence for both extensive coalescence and multiple stages of vesiculation. Additional factors responsible for the shape of these distributions include the high vesicularities of pumice clasts and large range of vesicle sizes, which impose mass balance constraints (Blower et al. 2001) and the steady-state assumption of constant bubble growth rate, which does not apply to a decompressing magma.

The same data used to calculate VSDs can be presented as vesicle volume distributions (e.g., Klug and Cashman 1994) or as power law plots of vesicle number as a function of size (Gaonac'h et al. 1996a, 1996b; Blower et al. 2001). Where ln *n* vs. L plots (e.g., Fig. 7) are strongly non-linear (and cannot be reduced to simple descriptors of dominant size and number density), these alternative presentations of the textural data allow more quantitative interpretation of vesicle populations.

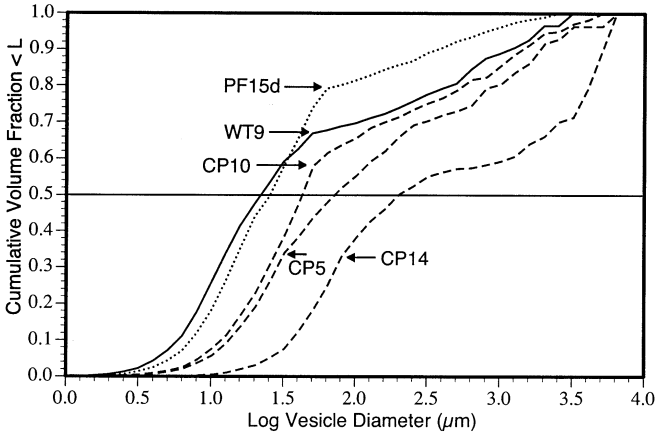

Fig. 9 Volume distributions of representative samples plotted as the cumulative volume < vesicle diameter L. Intersection of curves with the horizontal line at 0.5 denotes the volume-based median vesicle size. *Arrows* point to the change in slope in the volume distribution which marks the boundary between the dominant mode of small vesicles and larger coalesced vesicles

Vesicle volume distributions

Vesicle volume distributions (Fig. 8) are typically polymodal. Polymodal vesicle volume distributions have been variably attributed to multiple stages of bubble nucleation and growth (Sparks and Brazier 1982; Whitham and Sparks 1986) and to bubble coalescence (Orsi et al. 1992; Klug and Cashman 1996; Mangan and Cashman 1996). With one exception (CP14), volume distributions shown in Fig. 8 have dominant peaks (modes) at small vesicle diameters and subordinate peaks at larger diameters. These distributions suggest that most of the vesiculation occurred over a limited time and relatively late in the vesiculation history. Pumice clasts from the Plinian fall deposit can be distinguished from those of the pyroclastic-flow deposits on the basis of their larger modes (50–90 μm compared to 15–40 μm, respectively). Cumulative plots of the vesicle volume data allow direct comparison among representative samples (Fig. 9). Here volume-based median vesicle diameters (the diameter at a cumulative volume fraction of 0.5) vary by an order of magnitude, from 15–20 μm in pyroclastic-flow deposits to 200 μm in fall deposit sample CP14 (Table 1). Distri-

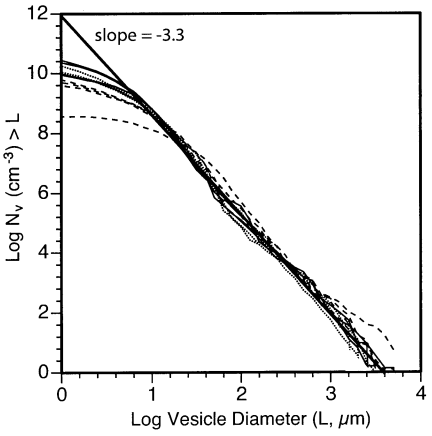

Fig. 10 Cumulative number densities (N_v>L). The *line* drawn has a slope of –3.3 and is the best fit to the large-vesicle data for all samples

bution shapes also vary. Near-unimodal volume distributions form sigmoidal curves with a constant slope over much of the volume (PF15d), whereas extremely polymodal volume distributions show several slope breaks (CP14). In general, pumice clasts from the Plinian fall deposit have more complex vesicle volume distributions than those of the Wineglass Welded Tuff and ring-vent-phase pyroclastic-flow deposits.

Cumulative number densities

Most important for comparison with experimental data are vesicle number densities, which represent the integrated result of bubble nucleation through time. Variations in vesicle number density are illustrated in Fig. 10, where the total number of vesicles larger than a given size (N>L) is shown as a function of vesicle size L. Here the number density of vesicles in a sample (per cm^3) is the intercept of each curve with log L=0 (where L is the vesicle diameter in μm, and 1 μm represents the small size limit of our imaging techniques). Vesicle number densities are referenced to the melt volume (N^m_V; Table 1) to account for differential expansion of individual bubble nuclei. Pumice clasts from the Plinian fall deposit have the lowest vesicle number densities, with N^m_V~5×10^9 cm^{-3}. Number densities in clasts from pyroclastic flows of the Wineglass Welded Tuff (WT) and ring-vent phase (PF) are slightly higher on average, with N^m_V~1–2×10^{10} cm^{-3}.

Vesicle size distributions obeying power law behavior have recently been described in both basaltic (Gaonac'h et al. 1996a, 1996b) and silicic (Simakin et al. 1999; Blower et al. 2001) systems. Figure 10 shows that vesicle populations in Mazama clasts also define power law trends (linear distributions on Fig. 10). In fact, vesicle data from all clasts define a single power law trend with a slope of –3.3 (range –3.0 to –3.5), or average fractal dimension D=3.3. Plinian fall deposit samples have slightly lower D values than the average, whereas samples from the ring-vent-phase pyroclastic flows have slightly higher than average D values. All samples also deviate from the power law trend at small vesicle sizes where they define exponential trends (e.g., Blower et al. 2001). Together, the data suggest that vesicles preserved in all pumice clasts may be divided into two populations: small vesicles with exponential size distributions and unimodal volume distributions (the 'diffusion' population of Gaonac'h et al. 1996a), and large vesicles which follow power law systematics.

Discussion

Qualitative and quantitative observations on pumice clasts from the ca. 7,700 year B.P. eruption of Mount Mazama provide a glimpse into magmatic processes occurring during a large, caldera-forming eruption. Clast vesicularity and permeability are bulk properties which preserve information on vesicle packing and connectivity. Detailed measurements of vesicle size distributions can be used to determine the relative timing and importance of bubble nucleation, growth, and coalescence. Comparison of these data with recent experiments on bubble nucleation and growth in rhyolitic melts permits speculation on conditions of syn-eruptive vesiculation. Together, these observations may be combined to infer changes in conditions of vesiculation and fragmentation which may have accompanied the transition from the single-vent to the ring-vent phase of the Mazama eruption.

Vesicularity-permeability relationships

Vesicularity and permeability are bulk properties that are easily measured and provide information on gross pumice structure. The vesicularity of all Mazama samples is high (≥75%), as is common for the products of silicic explosive eruptions (e.g., Houghton and Wilson 1989; Klug and Cashman 1996; Gardner et al. 1996). The range in vesicularity (75–88%) is consistent with predictions for closest packing of polydisperse (multisized) spheres (Sparks 1978; Cashman and Mangan 1994). Clast vesicularity does not approach the very high values (>90%) predicted for equilibration with atmospheric pressure (Thomas et al. 1994), nor is there evidence of differential expansion across clasts, as anticipated for post-fragmentation expansion (e.g., Kaminski and Jaupart 1997). Therefore, it appears likely that the vesicularity of most pumice clasts records the state of the magma at some pressure in excess of atmospheric, most likely that near the fragmentation level (Sparks 1978).

Pumice permeability is not a predictable function of bulk vesicularity (Fig. 4). Pumice clasts from the Plinian fall deposit have consistently high permeabilities that reflect the high interconnectivity of the vesicle structure (Fig. 3). Percolation theory (e.g., Sahimi 1994) predicts a

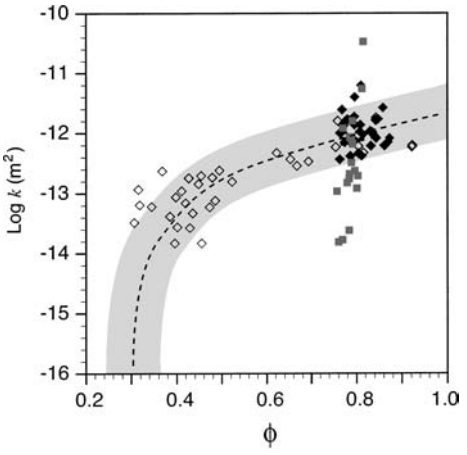

Fig. 11 Porosity-permeability curves for pumice from the Plinian fall deposit (*closed diamonds*), from the pyroclastic flow deposits (*shaded squares*), and from Klug and Cashman (1996; *open diamonds*). The *shaded band* shows one-half log unit variation from the permeability curve shown as *dashed line*

power law relationship between permeability (k) and porosity (vesicle volume fraction, ϕ) of the form

$$k(\phi) = c(\phi - \phi_{cr})^{\mu}, \quad (1)$$

where c is a constant that determines permeability magnitude, ϕ_{cr} is the critical porosity or the percolation threshold (the minimum ϕ at which a connected pathway exists across a bubble network), and exponent μ is controlled by the percolation pathway geometry. For voids modeled as fully penetrating spheres, μ=2 and ϕ_{cr}=0.3 (Saar and Manga 1999). Figure 11 shows our data, together with those of Klug and Cashman (1996), compared with a percolation curve. Most of the Plinian fall data can be modeled using Eq. (1) if c is varied to include an envelope (shaded in Fig. 11) of approximately one log unit. Here we have not normalized the permeability to the characteristic vesicle cross-sectional area (e.g., Saar and Manga 1999; Blower 2001) because we did not do textural measurements on all of the samples and the vesicle populations in the samples analyzed are sufficiently heterogeneous that a single characteristic cross-sectional area was difficult to determine. Normalization of the measurements could decrease the observed variability.

Permeability can be related to pumice structure by considering the size and geometry of apertures connecting adjacent vesicles through application of the Kozeny-Carman relation (e.g., Berryman and Blair 1987; Saar and Manga 1999):

$$k = \phi a^2 / C, \quad (2)$$

where a is the average hydraulic radius of the vesicle apertures, and C is a geometric constant (=2 for cylinders). Our imaging indicates that pumice clasts from the Plinian fall deposit have aperture diameters of 2–10 μm, consistent with measurements in other Plinian pumice samples (Sparks and Brazier 1982; Whitham and Sparks 1986). When used in Eq. (2), a=1–5 μm yields permeabilities of 4×10^{-13} to 10^{-11} m^2 for ϕ=0.8 and C=2. These values bracket the observed values, confirming Saar and Manga's (1999) observation that aperture size, not vesicle size, controls permeability in vesicular samples.

Pumice clasts from the pyroclastic-flow deposits exhibit a wide range in permeability over a narrow range of vesicularities, forming a trend on Fig. 11 that crosses the percolation curve at a high angle and extends well beyond the envelope encompassing clasts from the Plinian fall deposit. This trend can be explained using two different characteristics of the pyroclastic-flow clasts. High permeabilities (up to 3.3×10^{-11} m^2) measured along the elongation axis of tube vesicles in the Wineglass Welded Tuff can be modeled using Eq. (2) by assuming that the small volume fraction (~0.1) of large (a>25 μm) elongated vesicles controls the bulk permeability. By contrast, low permeabilities measured in the ring-vent-phase pyroclastic-flow samples can be partially, but not completely, explained by their lower vesicle interconnectivity (Fig. 3). An average interconnected ϕ=0.7 and a=1 μm yields observed average permeabilities of 3×10^{-13}, whereas a=0.25 μm is required to explain the lowest measured permeabilities (2×10^{-14} m^2). Both the relatively low vesicle interconnectivity and the small average aperture sizes estimated from the permeability data suggest limited coalescence and aperture formation in the pyroclastic-flow samples. Finally, the correspondence between measured permeabilities and clast textures suggests that later, cooling-related fractures probably play a limited role in determining the permeabilities of most pumice clasts (e.g., Klug and Cashman 1996).

Pumice clast textures

Differences in pumice structure inferred from vesicularity and permeability measurements are quantified through textural analysis of the preserved vesicle population. Vesicle size distributions are the integrated result of bubble nucleation, growth, and coalescence. Here we attempt to unravel the vesiculation histories preserved in Mazama pumice clasts through use of the vesicle size projections presented above. We relate vesicle number densities to those of relevant experiments to estimate rates of nucleation. We then show that vesicle volume distributions may be used to identify vesicles produced during the main phase of nucleation and use observed power law curves to support qualitative evidence of extensive bubble coalescence.

Bubble nucleation

Vesicle number densities record the integrated bubble nucleation and growth history of a sample. Melt-referenced (N^m_V) number densities are high ($1–20\times10^9$ cm^{-3}). Although bubble nucleation rates cannot be calculated directly from these data as nucleation times are not con-

strained, rates can be inferred using experimental data. Bubble nucleation experiments show both heterogeneous nucleation on container walls or on existing crystals and homogeneous nucleation in sample interiors. Both heterogeneous and homogeneous nucleation can yield high bubble number densities (~10^8 cm^{-3}; Hurwitz and Navon 1994; Lyakhovsky et al. 1996; Gardner et al. 1999; Mangan and Sisson 2000), particularly when volatile contents are high (7 wt% H_2O, ~600–700 ppm CO_2) and supersaturations exceed 110–120 MPa (Mourtada-Bonnefoi and Laporte 1999).

Based on these experiments and the apparent absence of heterogeneous nucleation sites (e.g., microlites), we interpret the high vesicle number density of the pumice clasts to result from homogeneous bubble nucleation at high supersaturations (ΔP>120 MPa). Experimental constraints provide minimum nucleation rate estimates of 10^6–10^7 cm^{-3} s^{-1} and suggest that the observed vesicle number densities could be generated in 100–1,000 s, an estimate similar to the 300–1,200 s estimated for magma ascent and fragmentation in the 1991 caldera-forming eruption of Mount Pinatubo (Polacci et al. 2001). These vesicle number densities also provide potential input for calculation of (1) rates of bubble growth (Proussevitch and Sahagian 1998; Liu and Zhang 2000), (2) time scales for development of depletion shells around individual bubbles which may enhance brittle fragmentation in ascending magma (Zhang 1999; Lensky et al. 2001), and (3) inter-bubble diffusion distances necessary for maintenance of equilibrium during degassing (e.g., Gardner et al. 1999; Mangan and Sisson 2000).

Bubble growth and coalescence

After nucleation, bubbles grow by diffusion, expansion, and coalescence. The extent to which coalescence, rather than single bubble growth, was responsible for the final vesicle population in the pumice samples can be assessed from the distribution of bubble sizes. Bubble growth following a single nucleation event will result in a unimodal (Poisson) bubble population with a narrow size distribution and mode that shifts to larger values as bubbles grow (Lyakhovsky et al. 1996; Gardner et al. 1999). Inspection of Fig. 8 shows that all pumice clasts are characterized by a rather broad mode at vesicle diameters of 20–40 μm which encompasses from 35% (CP5, CP14) to 80% (PF15d) of the total vesicle volume (Fig. 9). Either multiple nucleation events or coalescence could explain this component of the vesicle population.

The effect of coalescence on bubble size distributions has been modeled assuming a cascade of binary coalescence events, which produces a power law distribution of bubble sizes with a fractal dimension D>3 (Gaonac'h et al. 1996a). Power law distributions can also be generated by continuous nucleation, as seen in slow decompression of silicic melts (Simakin et al. 1999). Here successive nucleation events permit bubbles to nucleate only in spaces between existing bubbles and, ideally, produce an 'Apollonian' packing structure with D=2.45 (Blower et al. 2001). Comparison of sequential nucleation simulations of Blower et al. (2001) with our data shows that the size distribution of the smaller vesicles (<~30–40 μm) in Mazama pumice is exponential, not power law, in form. This population apparently formed by rapid nucleation (and a small number of nucleation events) shortly before quenching. At bubble growth rates of 10^{-5} to 10^{-4} cm s^{-1} (Lyakhovsky et al. 1996; Mangan and Sisson 2000), growth of these nuclei to observed sizes of 20–40 μm could occur in 10s to 100s of seconds. Thus, we suggest that the dominant mode of the vesicle size distributions is primarily the result of bubble nucleation and growth during magma ascent and just prior to clast quenching.

The larger vesicle population (diameters>~40 μm) is best fit by a power law distribution with D=3.3, a value significantly higher than the Apollonian value of 2.45 for continuous nucleation. This power law exponent suggests that the large vesicle population was produced by coalescence of smaller bubbles after an initial period of nucleation and growth. That coalescence was occurring up to the time of clast quenching is indicated by the preservation of incipient melt rupture and retraction, as shown by the wrinkling of viscous melt films around apertures (e.g., Figs. 5, 6).

Melt thinning and rupture were most likely driven by both decompression and pressure differences between bubbles (e.g., Klug and Cashman 1996). Internal bubble pressure ΔP is $2\sigma/r$, where σ is surface tension and r is bubble radius (Sparks 1978). When small bubbles from the population mode (r=10–20 μm) expand into larger (previously coalesced) bubbles (r=80–100 μm), ΔP may approach 20,000 Pa, assuming σ=0.1 N m^{-1} (Mangan and Sisson 2000). The time of film thinning (t) may be calculated from

$$t = \left[3\eta R_c^2 / 2\Delta P\right]\left[1/\delta_f^2 - 1//\delta_i^2\right] \quad (3)$$

where η is viscosity, R_c is the radius of the thinning film disc, δ_i is the initial film thickness, and δ_f is the final film thickness. For η=10^6 Pa s, R_c=10^{-5} m, δ_i=10 μm and δ_f=1 μm, ΔP=20,000 Pa yields a film thinning time of 1.5×10^4 s. The additional driving force created by decompression and bubble expansion would greatly reduce this estimate of film thinning time. Taken together, these observations suggest that the vesicle textures preserved in pumice probably required 10^2–10^4 s to develop, and that clasts which experience shorter times between initiation of bubble nucleation and clast quenching should show less coalescence than clasts with protracted expansion histories.

Finally, some large bubbles may have been inherited from the magma storage area (e.g., Whitham and Sparks 1986). Early bubbles are difficult to identify unambiguously. The most likely candidates for pre-existing bubbles are anomalously large vesicles that perturb the vesicle volume distributions (Fig. 8). Inherited bubbles may also be recognized where vesicles of different sizes appear to have experienced very different strain histories

(e.g., Fig. 6e, f), although this feature could equally result from multiple stages of bubble nucleation in the conduit. Nowhere do we see evidence of local volatile (and vesicle) depletion which characterizes inherited bubbles in experiments (Gardner et al. 1999; Larsen and Gardner 2000). Thus we conclude that although some small fraction of the larger bubbles may have been inherited from the magma storage area, much of the large vesicle population is best explained by coalescence.

Implications of pumice textures for fragmentation processes

Information provided by measurements of bulk properties and pumice textures presented above can be combined to examine general processes related to fragmentation during the Mazama eruption. The high number density and single mode of the smaller vesicle population suggests that the dominant phase of vesiculation involved homogeneous nucleation at high supersaturation. Rapid growth and expansion of earlier-formed bubbles resulted in bubble coalescence and extensive permeability development prior to quenching. We suggest that this sequence of events is most consistent with nucleation triggered by downward propagation of a decompression wave, followed by bubble expansion, bulk magma acceleration, and disruption (e.g., Mader et al. 1994, 1996; Papale 1999; Martel et al. 2000). The small vesicle population shows little bubble elongation, as might be anticipated from rapid magma expansion. However, preserved bands of highly deformed vesicles indicate that strain was probably localized. Deformed packets of long-tube vesicles also indicate complex strain histories. Thus the strain history during magma ascent is not easily inferred from bubble deformation in a single pumice clast, except where the strain has been equally distributed (as in the case of long-tube pumice).

Near-constant permeabilities in pumice from the Plinian fall deposit reflect the high pore interconnectedness of these samples (>95%) and well-developed vesicle apertures (a>1–5 μm). That this permeability range appears characteristic of Plinian pumice deposits in general suggests that permeabilities of $\approx 10^{-12}$ m^2 may be required to prevent total disruption of vesicular magma under Plinian eruption conditions (Klug and Cashman 1996). By contrast, pumice clasts from the ring-vent-phase pyroclastic-flow deposit have low permeabilities (10^{-13}–10^{-14} m^2). These permeabilities can be modeled using the observed low interconnected vesicularity combined with small pore apertures (a=1 μm). Both of these characteristics are consistent with vesicle size measurements, which suggest that as little as 20% of the vesicle volume may result from coalescence (Fig. 9).

Although our sampling was representative rather than comprehensive, these differences in the structure and permeability of clasts from the Plinian fall and pyroclastic-flow deposits suggest relationships between changes in eruptive conditions and resultant pumice textures. In

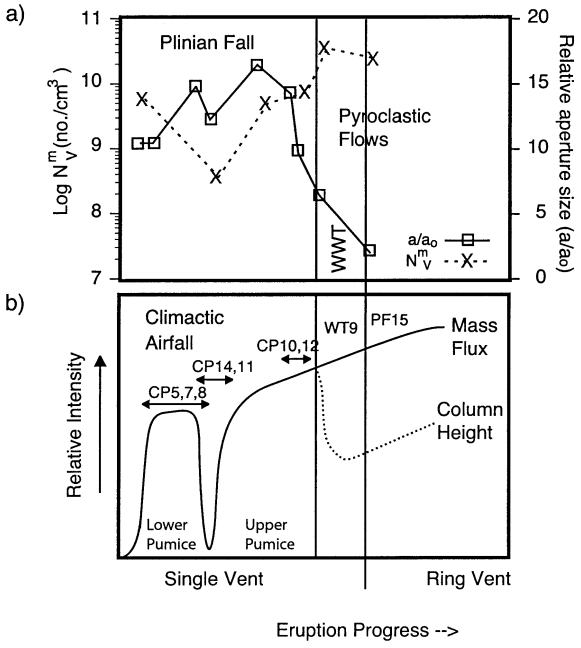

Fig. 12 **a** Melt-referenced vesicle number densities (N^m_V) and calculated pore aperture ratios (assuming a reference a_o=0.1 μm) shown as a function of eruption progress. *Vertical lines* separate the three phases of the eruption (Plinian fall, Wineglass Welded Tuff, ring-vent-phase pyroclastic flows). **b** Schematic portrayal of patterns of eruption column height and eruption velocity throughout the Plinian and pyroclastic flow phases of the Mazama eruption (based on Bacon 1983; Young 1990)

Fig. 12a we show changes in average vesicle number density (N^m_V) throughout the Mazama eruption. We could as well have shown vesicularity or median vesicle size, as both are inversely proportional to N^m_V. Also shown are relative mean vesicle aperture sizes (a/a_o) inferred from the minimum pumice permeabilities referenced to an initial aperture size a_o=0.1 μm. We use minimum values here to eliminate anisotropic effects of large elongated vesicles. Figure 12b shows a schematic representation of changes in eruption conditions inferred from detailed studies of the eruptive deposits (Bacon 1983; Young 1990). Here column height is assumed to be proportional to mass flux during the climactic Plinian phase. The inferred drop in column height in the middle of the Plinian phase marks a brief pause in activity between deposition of the Lower and Upper fall units (Young 1990). The increase in mass flux in the late Plinian and through the Wineglass Welded Tuff phase is inferred from increasing instability of the eruption column, which resulted in minor intra-Plinian pyroclastic flows and eventually column collapse (Bacon 1983; Kamata et al. 1993; Suzuki-Kamata et al. 1993). Extensive vent widening during the ring-vent phase of the eruption was accompanied by sufficient increase in column height (mass eruption rate) to generate pyroclastic flows which surmounted topographic highs not crossed by pyroclastic flows of the Wineglass Welded Tuff (Bacon 1983).

N^m_V appears roughly proportional to inferred mass flux and correlates inversely with vesicle aperture size (permeability and vesicle interconnectedness). Moderate volumetric eruption rates throughout most of the single-vent Plinian phase of the eruption produced pumice clasts with $N^m_V < 10^{10}$ cm^{-3}, a/a_o=10–15 μm, permeabilities ≈10^{-12} m^2, and intermediate vesicle sizes (volumetric modes ~30–50 μm). These textural and physical characteristics appear typical of Plinian fall deposits (e.g., Toramaru 1990; Klug and Cashman 1994, 1996) and require sufficient time between bubble nucleation and fragmentation for extensive coalescence. That bubble expansion and coalescence occurred before (or during) fragmentation and not afterward is suggested by the heterogeneity of vesicle textures within and between clasts – free expansion of an isolated clast should result in a radial symmetry to the vesicle textures. Additionally, clasts lack evidence for differential cooling and expansion from interior to exterior margins.

A decrease in N^m_V in the middle of the Plinian fall deposit corresponds to pumice clasts with a wider range in vesicle size and slightly higher vesicularities than clasts produced earlier or later in the Plinian sequence. These changes in vesicle characteristics do not result in increased permeability, however, consistent with Saar and Manga's (1999) conclusion that permeability is controlled by vesicle aperture size, not vesicle size. The apparent change in pumice structure in this part of the deposit may reflect the inferred decrease in eruption rates between deposition of the Lower and Upper pumice units (e.g., Young 1990), although verification of this interpretation would require much more extensive sample analysis.

Pumice clasts from eruptive phases that produced pyroclastic flows differ from those of the fall deposit in having generally higher vesicle number densities, lower clast vesicularities and permeabilities, and smaller minimum aperture sizes. These characteristics suggest both high rates of decompression and limited time for bubble growth and coalescence prior to fragmentation and quenching. Based on these data, we suggest that the high mass eruption rates (>10^9 kg s^{-1}; Young 1990) inferred for the ring-vent (caldera collapse) phase of the eruption may have involved either an increase in eruption velocity or an increase in the depth of the fragmentation surface. Either change would result in a shorter available time between decompression and fragmentation.

Finally, large elongated vesicles in pumice of the Wineglass Welded Tuff appear to have had a more complex deformation history than surrounding groundmass vesicles and may represent bubbles inherited from the magma storage reservoir. Late-stage expansion recorded in these samples (Fig. 6f) reflects their hot depositional environment (comparatively low-mobility flows confined by topography), as does extensive melt film retraction recorded in large vesicle walls (Fig. 5f). The high permeability of clasts in this deposit would have increased the efficiency of gas escape, and thus aided welding (Sparks et al. 1999).

Using vesicularity and permeability as a proxy for textural measurements

Obtaining textural data on pumice samples is time consuming and difficult. Thin vesicle walls are fragile and easily damaged during processing, vesicles vary widely in size and must therefore be imaged using many different magnifications, and vesicle shapes are often irregular and poorly approximated by either spheres or ellipsoids, thus making stereological conversions inaccurate (Sahagian and Proussevitch 1998). One motivation of this study was to investigate the sensitivity of bulk pumice measurements, such as vesicularity and permeability, to observed variations in vesicle structure. We conclude that bulk measurements capture important aspects of pumice structure. However, we note that clast density alone is not sufficient to distinguish textural differences and that additional measurements, such as permeability and pycnometry, are required to discriminate different textural types. For example, Mazama ring-vent-phase pyroclastic-flow samples have bulk vesicularities that are similar to those of the fall deposit, but are distinguished by their relatively high proportion of isolated pores (~10%), anomalously low permeabilities, and small estimated vesicle aperture diameters. Texturally, these clasts have higher number densities and a smaller volumetric proportion of coalesced vesicles than pumice from the Plinian fall deposit. Thus, the bulk measurements and textural measurements provide similar evidence of high nucleation rates and modest post-nucleation modifications to the bubble population.

Finally, we conclude that both vesicle interconnectivity and vesicle aperture size may influence permeability. These relationships could be tested by combining porosimetry with the bulk measurement techniques used here. For example, published porosimetry measurements of pumice clasts from pyroclastic-fall and flow deposits (Sparks and Brazier 1982; Whitham and Sparks 1986) suggest textural differences between paired fall and flow samples (from different phases of the same eruption) which are consistent with the differences shown in this study. All fall deposit clasts analyzed by porosimetry show two dominant modes in the vesicle volume distribution, one at vesicle diameters of 15–25 μm, the other at 80–180 μm. By contrast, analyzed clasts from pyroclastic-flow deposits show only one mode at 10–20 μm. Both clast types have an additional mode at 2 μm which can be attributed to vesicle apertures. These textural differences suggest that pumice produced during Plinian stages of an eruption typically shows more extensive coalescence than pumice produced during ignimbrite phases. Although the data are limited, they suggest that fundamental changes in rates or styles of decompression and fragmentation may occur as eruptions transition from high columns to caldera formation.

Conclusions

In our study of pumice clasts produced during both the single and ring-vent phases of the ca. 7,700 year B.P. eruption of Mount Mazama, we have shown that bulk measurements of pumice density (vesicularity) and permeability can provide important information on conditions of fragmentation and eruption. Pumice clasts from Plinian phases of the Mazama eruption are similar to silicic pumice from other Plinian fall deposits in having vesicularities of 75–85% and permeabilities of 0.5–5× 10^{-12} m^2. These data, together with those of similar studies (e.g., Klug and Cashman 1994, 1996) suggest that conditions leading to fragmentation of rhyolitic melt, and preservation of pumice during this process, are similar in eruptions of varying magnitude and intensity (eruptions of VEI~5–7). The apparent insensitivity of bulk properties to inferred variations in mass flux suggests that eruption velocities may be similar for a range of mass flux conditions, an inference most consistent with bubble nucleation controlled by downward propagation of a decompression wave and fragmentation resulting from subsequent expansion and acceleration of the bubbly melt. Measured clast permeabilities can be modeled by percolation theory (e.g., Saar and Manga 1999) and suggest that permeability is controlled primarily by the size of vesicle apertures created during extensive bubble coalescence.

Our interpretation of fragmentation conditions is supported by detailed textural analysis of individual pumice clasts. Most clasts have high (melt-referenced) vesicle number densities (~10^9–10^{10} cm^{-3}) which appear consistent with rapid nucleation (10^6–10^7 cm^{-3} s^{-1}) at high supersaturations (ΔP>120 MPa). Post-nucleation modifications to bubble populations include bubble growth by diffusion, expansion, and bubble-bubble coalescence. Bubble growth following rapid nucleation can account for up to 80% of the vesicle population in some clasts. This unimodal vesicle population accounts for a higher percentage of the total vesicle volume in clasts from the pyroclastic-flow deposits than in those from the fall deposits. These clasts also show less overall bubble growth (smaller mode and median sizes), less coalescence, smaller vesicle apertures, and a higher percentage of isolated vesicles. By contrast, pumice clasts from the fall deposit show multiple vesicle modes. Smaller vesicles have exponential distributions and modes of 20–40 μm. Larger vesicles have power law distributions with an average fractal dimension D=3.3. We interpret this power law signature to reflect bubble coalescence (Gaonac'h et al. 1996a) rather than continuous or sequential nucleation (Simakin et al. 1999; Blower et al. 2001) on the basis of both D>3 and abundant textural evidence for extensive coalescence. Additionally, some of the larger vesicles may have been inherited from the magma storage region, particularly those which deviate from simple power law distributions or where large bubbles have experienced different deformation histories from the matrix vesicles.

Finally, comparison of bulk (vesicularity and permeability) and detailed textural measurements suggests that bulk measurements capture many of the important components of the textural variations in pumice samples. As bulk measurements are much less time consuming than textural analysis of individual samples, comprehensive studies of pyroclastic deposits are probably best accomplished using these methods. We note, however, that density alone does not allow discrimination of different clast populations, and that both measurements of isolated pore volumes and clast permeabilities provide important additional information. Finally, near-complete characterization of bulk samples could be achieved by combining porosimetry with pycnometry and permeability measurements.

Acknowledgements The authors gratefully acknowledge reviews by M. Mangan and J. Lowenstern of an early version of the manuscript, and by O. Navon and H. Mader of a later version. They also acknowledge the National Park Service who gave permission for the sampling required by this study. This work was supported by NSF EAR9614753 and EAR9909507 to KVC.

References

Alidibirov M, Dingwell DB (2000) Three fragmentation mechanisms for highly viscous magma under rapid decompression. J Volcanol Geotherm Res 100:413–421

Bacon CR (1983) Eruptive history of Mount Mazama and Crater Lake caldera, Cascade Range, U.S.A. J Volcanol Geotherm Res 18:57–115

Bacon CR, Druitt TH (1988) Compositional evolution of the zoned calcalkaline magma chamber of Mount Mazama, Crater Lake, Oregon. Contrib Mineral Petrol 98:224–256

Bacon CR, Newman S, Stolper E (1992) Water, CO_2, Cl, and F in melt inclusions in phenocrysts from three Holocene explosive eruptions, Crater Lake, Oregon. Am Mineral 77:1021–1030

Berryman JG, Blair SC (1987) Kozeny Carmen relations and image processing methods for estimating Darcy's constant. J Appl Phys 62:2221–2228

Blower JD (2001) Factors controlling permeability-porosity relationships in magma. Bull Volcanol 63:497–504

Blower JD, Keating JP, Mader HM, Phillips JC (2001) Inferring volcanic degassing processes from vesicle size distributions. Geophys Res Lett 28:347–350

Cashman KV, Mangan MT (1994) Physical aspects of magmatic degassing II. Constraints on vesiculation processes from textural studies of eruptive products. Rev Mineral 30

Cashman KV, Marsh BD (1988) Crystal size distribution (CSD) in rocks and the kinetics and dynamics of crystallization II. Makaopuhi lava lake. Contrib Mineral Petrol 99:292–305

Cashman KV, Sturtevant B, Papale P, Navon O (2000) Magmatic fragmentation. In: Sigurdsson H (ed) Encyclopedia of volcanoes. Academic Press, New York, pp 421–430

Debregeas G, deGennes P-G, Brochard-Wyart F (1998) The life and death of "bare" viscous bubbles. Science 279:1704–1707

Druitt TH, Bacon CR (1986) Lithic breccia and ignimbrite erupted during the collapse of Crater Lake caldera, Oregon. J Volcanol Geotherm Res 29:1–32

Druitt TH, Bacon CR (1989) Petrology of the zoned calcalkaline magma chamber at Mount Mazama, Crater Lake, Oregon. Contrib Mineral Petrol 101:245–259

Gaonac'h H, Lovejoy S, Stix J, Schertzer D (1996a) A scaling growth model for bubbles in basaltic lava flows. Earth Planet Sci Lett 139:395–409

Gaonac'h H, Stix J, Lovejoy S (1996b) Scaling effects on vesicle shape, size and heterogeneity of lavas from Mount Etna. J Volcanol Geotherm Res 74:131–153

Gardner JE, Thomas RME, Jaupart C, Tait S (1996) Fragmentation of magma during Plinian volcanic eruptions. Bull Volcanol 58:144–162
Gardner J, Hilton M, Carroll MR (1999) Experimental constraints on degassing of magma: isothermal bubble growth during continuous decompression from high pressure. Earth Planet Sci Lett 168:201–218
Gilbert JS, Sparks RSJ (1998) The physics of explosive volcanic eruptions. Geol Soc Lond Spec Publ 145
Houghton BF, Wilson CJN (1989) A vesicularity index for pyroclastic deposits. Bull Volcanol 51:451–462
Hurwitz S, Navon O (1994) Bubble nucleation in rhyolitic melts: Experiments at high pressure, temperature, and water content. Earth Planet Sci Lett 122:267–280
Kamata H, Suzuki-Kamata K, Bacon CR (1993) Deformation of the Wineglass Welded Tuff and the timing of caldera collapse at Crater lake, Oregon. J Volcanol Geotherm Res 56:253–266
Kaminski E, Jaupart C (1997) Expansion and quenching of vesicular magma fragments in Plinian eruptions. J Geophys Res 102:12817–12203
Kaminski E, Jaupart C (1998) The size distribution of pyroclasts and the fragmentation sequence in explosive volcanic eruptions. J Geophys Res 103:29759–29779
Klug C, Cashman KV (1994) Vesiculation of May 18, 1980 Mount St. Helens magma. Geology 22:468–472
Klug C, Cashman KV (1996) Permeability development in vesiculating magma. Bull Volcanol 58:87–100
Larsen JF, Gardner J (2000) Experimental constraints on bubble interactions in rhyolite melts: implications for vesicle size distributions. Earth Planet Sci Lett 180:201–214
Lensky NG, Lyakhovsky V, Navon O (2001) Radial variations of melt viscosity around growing bubbles and gas overpressure in vesiculating magmas. Earth Planet Sci Lett 186:1–6
Liu Y, Zhang Y (2000) Bubble growth in rhyolitic melt. Earth Planet Sci Lett 181:251–264
Lyakhovsky V, Hurwitz S, Navon O (1996) Bubble growth in rhyolitic melts: experimental and numerical investigation. Bull Volcanol 58:19–32
Mader HM et al. (1994) Experimental simulations of explosive degassing of magma. Nature 372:85–88
Mader HM, Phillips JC, Sparks RSJ, Sturtevant B (1996) Dynamics of explosive degassing of magma: observations of fragmenting two-phase flows. J Geophys Res 101:5547–5560
Mangan MT, Cashman KV (1996) The structure of basaltic scoria and reticulite and inferences for vesiculation, foam formation, and fragmentation in lava fountains. J Volcanol Geotherm Res 73:1–18
Mangan MT, Sisson T (2000) Delayed, disequilibrium degassing in rhyolite magma: decompression experiments and implications for explosive volcanism. Earth Planet Sci Lett 183:441–455
Mangan MT, Cashman KV, Newman S (1993) Vesiculation of basaltic magma during eruption. Geology 21:157–160
Martel C, Dingwell DB, Spieler O, Pichavant M, Wilke M (2000) Fragmentation of foamed silicic melts: an experimental study. Earth Planet Sci Lett 178:47–58
Marti J, Soriano C, Dingwell DB (1999) Tube pumices as strain markers of the ductile-brittle transition during magma fragmentation. Nature 402:650–653
Mourtada-Bonnefoi CC, Laporte D (1999) Experimental study of homogeneous bubble nucleation in rhyolitic magmas. Geophys Res Lett 26:3505–3508
Orsi G et al. (1992) A comprehensive study of pumice formation and dispersal: the Cretaio tephra of Ischia (Italy). J Volcanol Geotherm Res 53:329–354
Papale P (1999) Strain-induced magma fragmentation. Nature: 425–428
Polacci M, Papale P, Rosi M (2001) Textural heterogeneities in pumices from the climactic eruption of Mount Pinatubo, 15 June 1991, and implications for magma ascent dynamics. Bull Volcanol 63:83–97
Proussevitch AA, Sahagian DL (1998) Dynamics and energetics of bubble growth in magmas: analytical formulation and numerical modeling. J Geophys Res 103:18223–18251
Saar MO, Manga M (1999) Permeability-porosity relationship in vesicular basalts. Geophys Res Lett 26:111–114
Sahagian DL, Proussevitch AA (1998) 3D particle size distributions from 2D observations: stereology for natural applications. J Volcanol Geotherm Res 84:173–196
Sahimi M (1994) Applications of percolation theory. Taylor and Francis, London
Simakin A, Armienti P, Epel'baum MB (1999) Coupled degassing and crystallization: experimental study at continuous pressure drop, with application to volcanic bombs. Bull Volcanol 61:275–287
Sparks RJS (1978) The dynamics of bubble formation and growth in magmas: a review and analysis. J Volcanol Geotherm Res 3:1–37
Sparks RSJ, Brazier S (1982) New evidence for degassing processes during explosive eruptions. Nature 295:218–220
Sparks RSJ, Tait SR, Yanev Y (1999) Dense welding caused by volatile resorption. J Geol Soc Lond 156:217–225
Suzuki-Kamata K, Kamata H, Bacon CR (1993) Evolution of the caldera-forming eruption at Crater Lake, Oregon, indicated by component analysis of lithic fragments. J Geophys Res 98: 14,059–14,074
Tait S, Thomas R, Gardner J, Jaupart C (1998) Constraints on cooling rates and permeabilities of pumice in an explosive eruption jet from colour and magnetic mineralogy. J Volcanol Geotherm Res 86:79–91
Thomas N, Jaupert C, Vergniolle S (1994) On the vesicularity of pumice. J Geophys Res 99:15,633–15,644
Toramaru A (1990) Measurement of bubble size distributions in vesiculated rocks with implications for quantitative estimates of eruption processes. J Volcanol Geotherm Res 43:71–90
Underwood E (1970) Quantitative stereology. Addison-Wesley, Reading, Massachusetts
Walker GPL (1973) Explosive volcanic eruptions – a new classification scheme. Geol Rundsch 62:431–446
Whitham AG, Sparks RSJ (1986) Pumice. Bull Volcanol 48:209–223
Williams H (1942) The geology of Crater Lake National Park, Oregon. Carnegie Inst Washington Publ
Young SR (1990) Physical volcanology of Holocene airfall deposits from Mt. Mazama, Crater Lake, Oregon. Doctoral Thesis, University of Lancaster
Zhang Y (1999) A criterion for the fragmentation of bubbly magma based on brittle failure theory. Nature 402:648–650